Photoinduced Charge-Transfer Reaction between Pyrene and *N*,*N*′-Dimethylaniline on Silica Gel Surfaces

Guohong Zhang and J. Kerry Thomas*

Department of Chemistry and Biochemistry, University of Notre Dame, Notre Dame, Indiana 46556

A. Eremenko and T. Kikteva

Institute of Surface Chemistry, National Ukrainian Academy of Sciences, Prospect Nauki 31, 252022 Kiev, Ukraine

F. Wilkinson

Department of Chemistry, Loughborough University, Loughborough, Leicestershire, LE 11 3UT, UK

Received: June 16, 1997[⊗]

Photoinduced charge-transfer reactions between adsorbed pyrene and *N*,*N*′-dimethylaniline (DMA) in porous silica gel are examined by fluorescence quenching and transient absorption techniques. The quenching on silica surfaces is found to be diffusion controlled and gives rise to exciplex formation on silica surfaces. Such a Langmuir−Hinshelwood type of surface reaction is described quantitatively using a two-dimensional kinetics model. Surface diffusion of DMA is found to be thermally activated and related to the hydrogen-bonding interaction between DMA and the surface hydroxyl groups. Properties of exciplex emission such as the position of the maximum and the quantum yield are used to characterize the surface environment. Deactivation of the exciplex on silica surfaces via charge recombination is understood in terms of photoassisted electron-transfer theory. The low yield of ionic products from dissociation of the contact ion pairs of the exciplex $^1(Py^{\bullet-}DMA^{\bullet+})^*$ is attributed to the lack of solvation and the low mobilities of ionic species on the surface. It is found that coadsorption of alcohols facilitates the charge separation.

Introduction

Photoinduced charge transfer has drawn particular attention over the past 30 years due to its fundamental importance in various electron-transfer (ET) reactions in chemistry and biology. So far, extensive and systematic studies on ET processes have been conducted in homogeneous systems, including both the gas and the liquid phase.[1−8] In his early theoretical work, Marcus first showed that solvents, as a significant part of the reaction coordinates, play a major role in ET reactions in condensed phases.[1] With the introduction of solvent reorganization energy, the relationship between the reaction rates (ln *k*) and the free energy driving force ($-\Delta G$) is well-described by a parabolic energy gap law for most ET reactions in liquid solutions.[1] Subsequent studies by Miller and co-workers provided the first experimental evidence in support of the energy gap law.[3,4] It is found that the majority of the forward ET reactions (charge separation) lie in the normal region and most of the back ET reactions (charge recombination) are in the inverted region. Experiments in low-temperature organic glasses and solid polymers also demonstrate that the same principle applies equally well to solid solutions.[4,9] However, extension of the above successful approaches developed from the homogeneous systems to multiphase systems, particularly solid surfaces, is still an open question.

It is well-known that light-induced charge separation is the key process in heterogeneous photocatalysis. Early work in various organized and constrained media has found that micelles can be successfully used to enhance the ion radical production by tuning the charge on the micellar surfaces.[10] One of the motivations behind the recent photochemical studies in solid systems is to promote charge separation by making use of the unique properties of surface environments, such as high polarity, rigid orientation, and geometric constraint.[11] Kochi and co-workers have shown that charge-transfer ion pairs from photoexcitation of MV^{2+} and arene complexes are more stable within a zeolite supercage than in very polar solvents such as acetonitrile ($\epsilon = 37.5$).[12] Such a stabilization effect was evident from significantly longer lifetimes of the ion pairs due to the slower back ET. This is distinct from what is conventionally observed in the inverted region. In contrast, recent work by Miyasaka found that the same energy gap law is operative in a porous glass (pretreated at $T_a = 480$ °C) as in liquid solutions; i.e., it exhibits typical inverted region behavior.[13] The total reorganization energy for charge recombination of the contact ion pairs was estimated to be 0.36 eV. After deduction of the vibrational contribution, the surface reorganization energy is less than 0.1 eV. It is much smaller than that in a polar solution, indicative of a very limited environmental reorganization on the surface. The difference between the two solid systems above with regard to their influence on ET reactions calls for further investigation.

Silica gel is conventionally used as an inert support in most photochemical studies, and its surface has been well characterized in previous work. Photophysical studies with sensitive spectroscopic probes indicate that molecules adsorbed on silica surfaces sit in a polar environment.[14] Silica gel surfaces also exhibit a heterogeneous distribution of adsorption sites, which leads to nonexponential decay of the singlet excited state of a probe molecule.[15] The limited molecular motion across the silica surface makes bimolecular reactions between coadsorbates much less extensive than those in liquid solutions.[16] Cage

* To whom correspondence should be addressed.

[⊗] Abstract published in *Advance ACS Abstracts,* September 15, 1997.

S1089-5647(97)01983-4 CCC: $14.00

effects on geminate radical reactions on dry silica surfaces clearly demonstrate the confinement of reactions by the porous structure.[17] It is interesting to examine the effects of these unique features on ET reactions on the silica surface.

This work reports intermolecular ET quenching of the pyrene singlet excited state by *N*,*N*′-dimethylaniline (DMA) on silica gel surfaces and the surface effects on the charge recombination and charge separation within the ion pair exciplex $^1(Py^{\bullet-}DMA^{\bullet+})^*$. The well-established charge-transfer reactions between pyrene and DMA in liquid solutions have been used as a good model system for studying ET reactions in other nonhomogeneous media, such as micelles,[20] membranes,[21] and surfaces.[22] It is found in our experiments that the bimolecular quenching reaction in the adsorbed state is limited by the molecular diffusion on the surface. The formation of an exciplex is observed as the result of the quenching reaction. In competition with the exciplex fluorescence emission, triplet formation, internal conversion, and dissociation into free ions are other nonradiative pathways that deactivate the exciplex. Quantum yields of these processes are measured on surfaces pretreated at different temperatures. The results are understood using Marcus theory of photoassisted electron-transfer reactions.[2]

Experimental Section

Chemicals. HPLC grade solvents (obtained from Aldrich) such as pentane, cyclohexane, and methanol were used throughout this work. The aromatic probe and quencher used in this work, namely pyrene and *N*,*N*′-dimethylaniline, are adsorbed on the solid surfaces from their pentane solutions.

Several different types of porous silicas are used in this work. Granular Merck silica gel powders M100 (pore size 100 Å, surface area 300 m^2/g) and Davisil silica gel D60 (pore size 60 Å, surface area 480 m^2/g) are purchased from Aldrich Chemical. Wide pore Fractosil silica gel (made by Merck) with two different pore sizes F200 (pore 180 Å, area 150 m^2/g) and F500 (pore 420 Å, area 50 m^2/g) are kindly provided by Professor D. Avnir at the Hebrew University of Jerusalem. These silica gels are made via base-catalyzed hydrolysis and polymerization of silicate acid and widely used as model systems of porous silicas. The primary particles are continuously linked via surface condensation reactions into a rigid three-dimensional network interpenetrated by a multiconnected porous structure. Small amounts of ionic impurities such as Cl^- and SO_4^{2-} present in silica gel are washed out before thermal activation using distilled and doubly deionized water before use.

Sample Preparation. Silicas exposed to air exhibit surfaces that are covered by physically adsorbed water. Heat treatment of silica powders in a 150 °C oven overnight removes most of the physisorbed water and results in a fully hydroxylated surface with vicinal hydroxyl groups interacting with each other via hydrogen bonding. Further heat treatment at higher temperatures starts to remove chemisorbed water by a condensation reaction. FTIR spectroscopy shows that heating to 500 °C removes most of the hydrogen-bonded hydroxyls, and the surface is left with mainly isolated hydroxyls. The surface coverage of hydroxyl groups is ∼5.0 OH/nm^2 in 150 °C dried silicas, and it is reduced to ∼2.2 OH/nm^2 on 500 °C dried surfaces.[23]

Adsorption of organic molecules such as pyrene and DMA onto activated silica surfaces occurs via hydrogen-bonding interaction. Adsorption isotherms of pyrene and DMA were measured in cyclohexane, which were then used to control the loading and avoid the complication from possible aggregation. Silica powder was activated overnight in an oven with its temperature set at 150 or 500 °C. Dried silica samples (normally 0.3 g in weight for each sample) were protected from air by pentane. Specific amounts of pyrene and DMA were then added to each slurry sample in a vial. The vials were sealed and kept in a desiccator for 8 h before the removal of pentane by drawing a vacuum on the desiccator. Initial vacuum pumping was carried out to an extent that there is still some pentane left on the surface, and the samples were allowed to reach adsorption equilibrium which is assisted by the presence of a thin solvent layer. Each loaded sample was then quickly transferred to a thin (1 or 2 mm in thickness) quartz cell. Further vacuum pumping at 10^{-3} Torr for 3 h completely removes the solvent, leaving only pyrene and DMA on the surface. Two millimeter cells are used in the diffuse fluorescence measurements, while 1 mm cells are used in transient absorption measurements in a diffuse transmittance mode. UV−visible absorption and fluorescence emission of DMA adsorbed on silica surfaces pretreated at 150 and 500 °C show no loss of DMA during the extensive vacuum pumping.

Diffuse Transmittance and Reflectance. Absorption spectra of silica samples are taken in diffuse reflectance and transmittance modes on a Cary UV−visible spectrometer equipped with an integrating sphere attachment. Applicability of the Lambert−Beer approach to the diffuse transmittance is examined by making measurements on 1 mm thick D60 powder samples loaded with a known amount of perylene. Such experiments show that transmittance is more sensitive than reflectance, and it exhibits a linear relation against the probe concentration at low loadings. However, spectra with absorbance larger than 0.3 suffer a nonlinear distortion, and the Lambert−Beer approach is no longer valid.[24] This is particularly important for the transient absorption measurements on silica powder samples in laser photolysis experiments.

Fluorescence Spectroscopy. Both steady-state and time-resolved fluorescence spectroscopy are used to examine the polarity of surface environment and possible aggregation of probe molecules on silica surfaces. Steady-state fluorescence spectra are taken on a SLM-5000C spectrofluorimeter. The fluorescence quantum yields of pyrene and the pyrene−DMA exciplex at different DMA coverages were measured by using pyrene emission as a standard. The fluorescence yield of pyrene on silica gel surfaces are taken as 0.51 and 0.56 for pretreatment at 150 and 500 °C, respectively.[25] Fluorescence lifetimes of the exciplex and fluorescence quenching kinetics of pyrene on silica surfaces are measured by using a PRA nitrogen laser LN-100 (pulse width ∼0.3 ns) as the excitation source and a Hamamatsu microchannel plate PMT (R1644U) as the detector. The total system response is 0.5 ns.

Transient Absorption Spectroscopy. A Photonics nitrogen laser (UV-24) with a pulse width of 8 ns and output of 5 mJ at 337 nm is used as the excitation source. A pulsed Xe flash lamp is used to analyze the transient species. For granular silica gel with a lower scattering power, transient absorption is taken in the diffuse transmittance mode with samples held in 1 mm quartz cells. A diffuse reflectance setup is used for transient measurements of highly scattering alumina and zeolite samples in 2 mm quartz cells. The diffusely reflected probe light is collected by an optical fiber. Details of the time-resolved diffuse reflectance system have been published elsewhere.[26]

Results and Discussion

I. Quenching of Pyrene Fluorescence by DMA in Adsorbed State. For silica gel M100 dried at 150 °C, aggregation of pyrene occurs at a loading larger than 8.0×10^{-6} mol/g, which is clearly indicated by the fluorescence and excitation spectra of pyrene excimer resulting from the formation of ground-state dimer on the surface. This means that the adsorption sites for pyrene are not uniformly spread over the

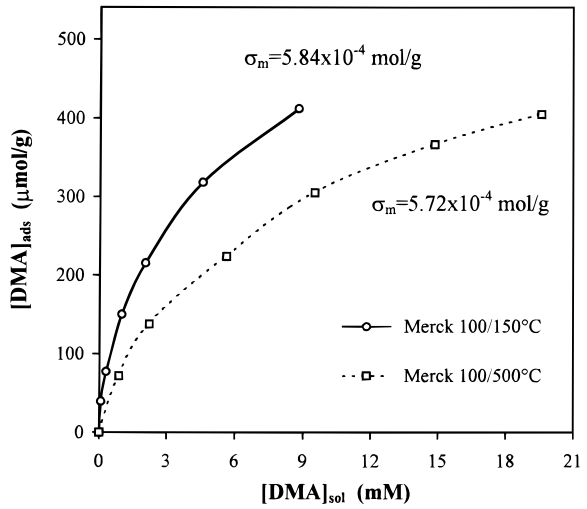

Figure 1. Adsorption isotherms of DMA on silica Merck 100 from cyclohexane solution. Silica samples are pretreated at 150 °C (solid line) and 500 °C (dash line).

entire available surface. Less than 10% of the surface is covered by pyrene before aggregation occurs. Further dehydroxylation of silica surface by thermal treatment at 500 °C reduces the number of such sites and leads to a significant aggregation above a pyrene loading of 2.0×10^{-6} mol/g. To avoid complications from effects of aggregation, low loading of pyrene around $(1.0-2.0) \times 10^{-7}$ mol/g is used throughout this work. In contrast to pyrene, DMA shows a fairly uniform adsorption on silica surfaces pretreated at different temperatures. Figure 1 shows the adsorption isotherms of DMA on silica surface adsorbed from cyclohexane solution. Measurements were made on two different surfaces pretreated at 150 and 500 °C, respectively. Neither of the adsorption isotherms can be fitted simply to the Langmuir equation, particularly in the low-concentration and low-loading regime. This is due to the heterogeneity of the adsorption sites. However, fitting the middle- and high-concentration portion of the isotherm to a Langmuir type of adsorption gives a monolayer coverage of $\sigma_m = 5.84 \times 10^{-4}$ mol/g. The area covered by a single DMA molecule is about 85 Å^2. In comparison with benzene, which is shown to have a molecular area of ~60 Å^2 on porous silica surface,[23] DMA might lie flat on the surface just like benzene. A similar adsorption pattern is also observed on the 500 °C treated surface. The monolayer coverage is slightly lower than that on the fully hydroxylated surface, $\sigma_m = 5.72 \times 10^{-4}$ mol/g. This can be understood by considering that there are still two hydroxyl groups available for adsorption within the molecular area of DMA (i.e., 85 Å^2) on the partially dehydroxylated surface. Different from the other large quencher molecules which tend to aggregate on the surface at adsorption levels well below the monolayer coverage,[16c] DMA exhibits a fairly uniform coverage of the silica surfaces. This enables us to describe surface bound DMA with a random distribution function and use a valid concept of surface concentration in modeling the fluorescence quenching kinetics.

Fluorescence measurements were made for a series of silica samples loaded with the same amount of pyrene (1.3×10^{-7} mol/g) and different amounts of DMA below monolayer coverage. Two different types of silica surfaces were also used to examine the effect of dehydroxylation on the quenching reaction. Figure 2a shows that the pyrene fluorescence is reduced with increased loading of DMA on the surface. The III/I ratio of the pyrene fluorescence fine structure (III/I = 0.62) does not change with the addition of DMA, indicating that pyrene is always adsorbed on the surface. Coadsorbed DMA

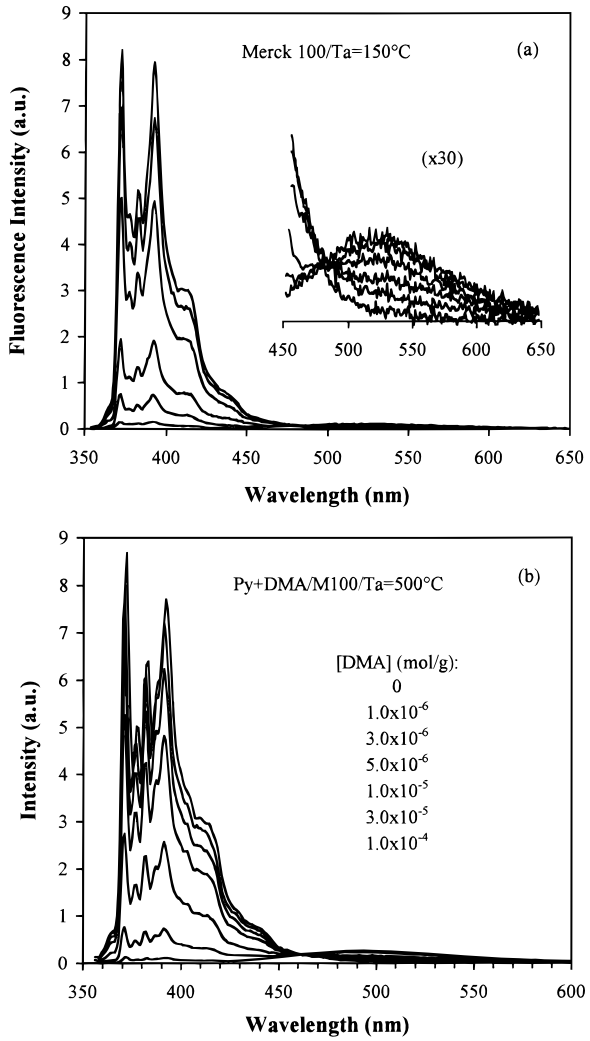

Figure 2. Steady-state measurements of pyrene fluorescence quenching by DMA on silica M100 surfaces pretreated at different temperatures. (a) $T_a = 150$ °C, [Py] $= 1.3 \times 10^{-7}$ mol/g, [DMA] $= 0$, 5.0×10^{-6}, 1.0×10^{-5}, 3.0×10^{-5}, 5.0×10^{-5}, and 1.0×10^{-4} mol/g. Insert shows the development of the exciplex emission spectrum in the longer wavelength region. (b) $T_a = 500$ °C, [Py] $= 1.3 \times 10^{-7}$ mol/g, [DMA] $= 0$, 1.0×10^{-6}, 3.0×10^{-6}, 5.0×10^{-6}, 1.0×10^{-5}, 3.0×10^{-5}, and 1.0×10^{-4} mol/g.

suppresses the pyrene emission spectrum in the 350−450 nm range, and another weak broad fluorescence band gradually appears around 520 nm. Based on well-established work in the liquid phase,[19] this green fluorescence is attributed to the exciplex produced from the bimolecular quenching reaction between the singlet excited-state pyrene ($^1Py^*$) and DMA. The $I_0/I \sim$ [DMA] plot with the intensity measured at 393 nm shows an upward curvature and is different from the Stern−Volmer type of linear plots observed in liquid solutions. The DMA loading at the 50% quenching of pyrene fluorescence is 1.5×10^{-5} mol/g, which corresponds to a volume concentration of about 11 mM (the pore volume of M100 is ~0.9 cm^3/g). A more efficient fluorescence quenching with the same nonlinear pattern is observed on the partially dehydroxylated surface. The DMA loading at the half quenching is 7.0×10^{-6} mol/g or 5.0 mM. In simple liquid solutions, the DMA concentration at half quenching is around 0.2 mM. It is found from the above steady-state results that pyrene and DMA react much less efficiently in the adsorbed state than in homogeneous solutions. The decrease in the pyrene fluorescence yield and the concomitant increase in the exciplex emission yield are clearly illustrated in Figure 3 with the DMA coverage changing from 0 to 1.0×10^{-4} mol/g on two different silica surfaces.

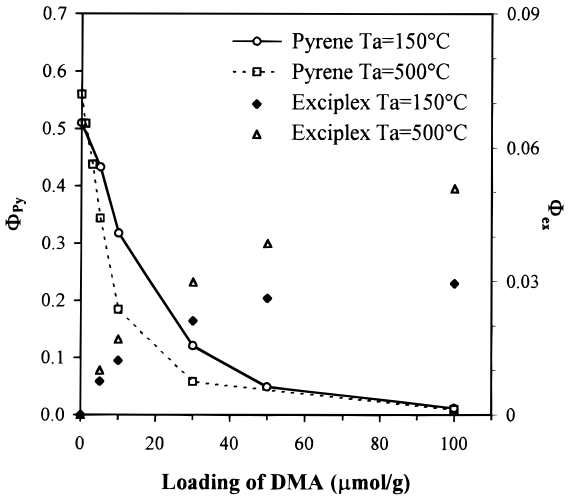

Figure 3. Fluorescence quantum yields of pyrene and the exciplex at different DMA loadings on fully hydroxylated and partially dehydroxylated silica surfaces.

Figure 4a illustrates the time-resolved fluorescence decay traces of pyrene measured on a fully hydroxylated surface as a semilog plot. It shows that the quenching is dynamic over the nanosecond time scale. No reduction in the fluorescence intensities measured at $t = 0.5$ ns (i.e., instrument response) is observed for silica samples with DMA loadings up to 10^{-4} mol/g. The absence of static quenching is indicative of no aggregation between pyrene and DMA and is in agreement with a uniform distribution of DMA molecules over the entire surface. The fluorescence quenching kinetics are nonexponential in all samples. In general, the decay in the presence of DMA consists of a nonexponential transient part in the short time scale and a fairly exponential decay at long times. Due to the contact nature of the charge-transfer reaction between $^1Py^*$ and DMA,[4a] it is reasonable to assume that diffusive motion of reactants is needed for the formation of a reactive encounter. This is later confirmed by the strong temperature effect on quenching kinetics; i.e., cooling shuts down the reaction. Therefore, the present system with both reactants in the adsorbed state provide a model system to study diffusion-controlled Langmuir−Hinshelwood reactions on silica surface.

If we consider that the charge-transfer interaction is only operative within a short distance of 7−8 Å[4a] and that there is no interaction between $^1Py^*$ and DMA separated by the 100 Å pore space within the same pore, then the reaction must involve diffusive motion of reactants on a folded surface. If we assume that the size of molecules is much larger than the surface roughness, the above Langmuir−Hinshelwood surface reaction can be treated as a two-dimensional system. It has been shown by Owen[27] and Doll[28] that, unlike the Smoluchowski approach to diffusion-limited reactions in a three-dimensional space, there is no steady-state solution to a two-dimensional diffusion problem. However, within a specific time range, the quenching kinetics can be well approximated by the following decay function.[27]

$$I(t) = I_0 \exp\{-k_0 t - 7.09\sigma_Q R_c\sqrt{Dt} - 1.59\sigma_Q Dt\} \quad (1)$$

where k_0 is the decay rate in the absence of quencher (s^{-1}), σ_Q is the surface concentration of the quencher (cm^{-2}), R_c is the encounter radius (cm), and D is the surface diffusion constant (cm^2/s). It has been shown numerically that the above approximation is only valid for time $t \leq 50R_c^2/D$. Within this time window, the decay function as described in eq 1 shows a transient behavior at short times and switches to an exponential decay in the long time regime. This has been successfully

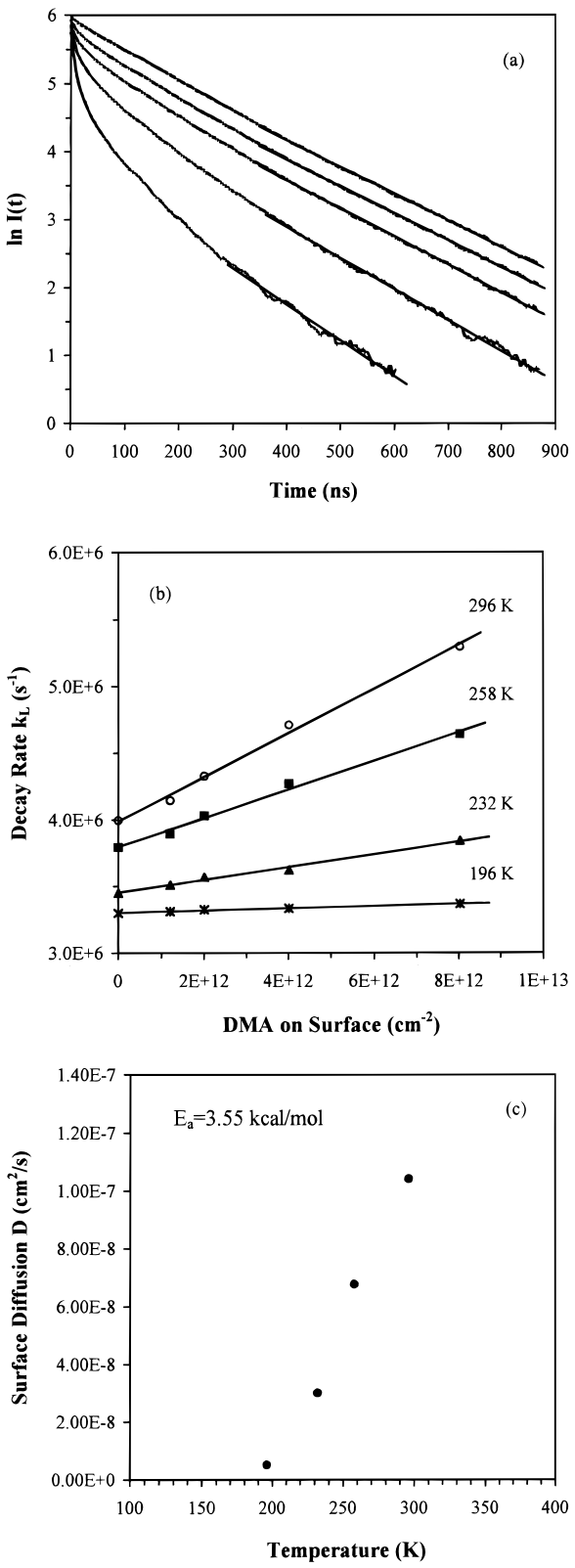

Figure 4. (a) Time-resolved measurements of pyrene fluorescence quenching by DMA on the fully hydroxylated silica M100 surface. Measurements were made at room temperature. The fluorescence intensity data are presented in a semilog plot. Straight lines are the linear regression of the long time kinetics. [Py] = 1.3×10^{-7} mol/g, [DMA] = 0, 5.0×10^{-6}, 1.0×10^{-5}, 3.0×10^{-5}, 5.0×10^{-5}, and 1.0×10^{-4} mol/g. (b) Increase of the long time decay rates with the surface concentration of DMA. Fluorescence quenching was measured at different sample temperatures. The data are fitted to a linear equation to abstract surface diffusion constants (see text). (c) Temperature dependence of the diffusion constant of DMA on M100 surface pretreated at $T_a = 150$ °C. Activation energy $E_a = 3.55$ kcal/mol is obtained from a linear regression of ln D against $1/T$.

applied to fluorescence quenching studies in two-dimensional monolayers and membranes.[21,29]

Direct application of eq 1 to the silica system is complicated by the nonhomogeneous decay of pyrene fluorescence which has been understood in a Gaussian model due to the site heterogeneity.[15] As shown in Figure 4a, the signal of pyrene fluorescence without any DMA loading deviates significantly from an exponential decay within the first 200 ns and quickly approaches the exponential on the long time scale (linear function in the semilog scale). This validifies the approach of applying eq 1 to describe the long time decay within the proper time window. As a result, the linear part of the decay traces in Figure 4a is used to abstract the long time decay rate k_L which is related to the quencher concentration in a linear relation.

$$k_L = k_0 + 1.59\sigma_Q D \qquad (2)$$

Fitting of the long time decay to a linear function on the semilog plot is illustrated in Figure 4a, which gives the value of k_L. Figure 4b shows the long time decay rates k_L at different DMA coverages and at different sample temperatures for the silica surface pretreated at 150 °C. A linear regression of k_L data against the DMA concentration leads to the diffusion constant D on the surface, e.g., $D = 1.04 \times 10^{-7}$ cm^2/s at room temperature, which corresponds to an apparent quenching rate constant of $k_q = 9.96 \times 10^{12}$ m^2 mol^{-1} s^{-1} according to $k_L = k_0 + k_q\sigma_Q$ for surface reactions. It is attributed to DMA movement on the surface, since pyrene is virtually immobilized on this time scale.[16c] Previous studies have shown that large aromatic molecules such as naphthacene and tetracene move much slower with their diffusion rates on the order of 10^{10} m^2 mol^{-1} s^{-1}.[30a] Compared with the movement of some small aromatic molecules on silica gel surface, the diffusion rate of DMA is close to those of naphthalene compounds[16] but is significantly faster than that of acridine.[30b] Recent studies of charge-transfer quenching of anthracene cation radicals by a series of electron donors on Davisil 60 (pore size 60 Å) surface suggest that the reaction rates are limited by the diffusion of quencher molecules across the surface.[30c] The quenching rate constant abstracted from a dispersive Gaussian kinetics model is $k_q = 7.20 \times 10^{12}$ m^2 mol^{-1} s^{-1} for DMA, which is very close the value measured in this work on M100 surface by the fluorescence quenching technique. The surface diffusion constant D is strongly affected by the temperature (Figure 4c). Analysis using the Arrhenius equation $D(T) = D_0 \exp\{-E_a/RT\}$ gives an activation energy of $E_a = 3.55$ kcal/mol, in agreement with a relatively strong hydrogen bonding of DMA to the silica surface.

Analysis of the time-resolved fluorescence quenching kinetics on the partially dehydroxylated M100 surface ($T_a = 500$ °C) shows that the surface diffusion constant of DMA is $D = 1.85 \times 10^{-7}$ cm^2/s, which is nearly twice as fast as that on the fully hydroxylated surface. Presumably, this results from a relatively weaker binding of DMA to silica and therefore a lower activation energy due to less available hydroxyl groups.

Similar fluorescence quenching kinetics is also observed in other silica gel samples, such as Davisil 60, Fractosil 200, and Fractosil 500. The III/I ratio of the pyrene fluorescence is III/I = 0.66 in the large pore Fractosil 500 pretreated at 150 °C, which is very close to that observed in the Merck silica M100. The exciplex emission has a maximum at 516 nm and a lifetime of 40 ns. The surface diffusion constant of DMA is measured to be 2.35×10^{-7} cm^2/s at room temperature from fitting the fluorescence decay traces to the two-dimensional kinetics. The significantly faster DMA diffusion in silica with large pores might be attributed to the effect of surface irregularity on the molecular movement. The above results are different from the earlier work by Avnir and co-workers,[22] who found, from their steady-state measurements, that the fluorescence quenching does not occur until DMA covers the entire surface. It was then proposed that the binding of DMA to the silica surface through the nitrogen atom does not allow DMA to achieve the proper configuration for the electron-transfer reaction with pyrene. Detailed comparison between the present work and the previous study shows that the major difference lies at the adsorption isotherms of DMA. In their work, the monolayer coverage occurs at a much lower DMA loading than what we have found in Figure 1. Time-resolved fluorescence measurements described in this work clearly demonstrate that fluorescence quenching is a dynamic process, and it even occurs at low coverages of DMA.

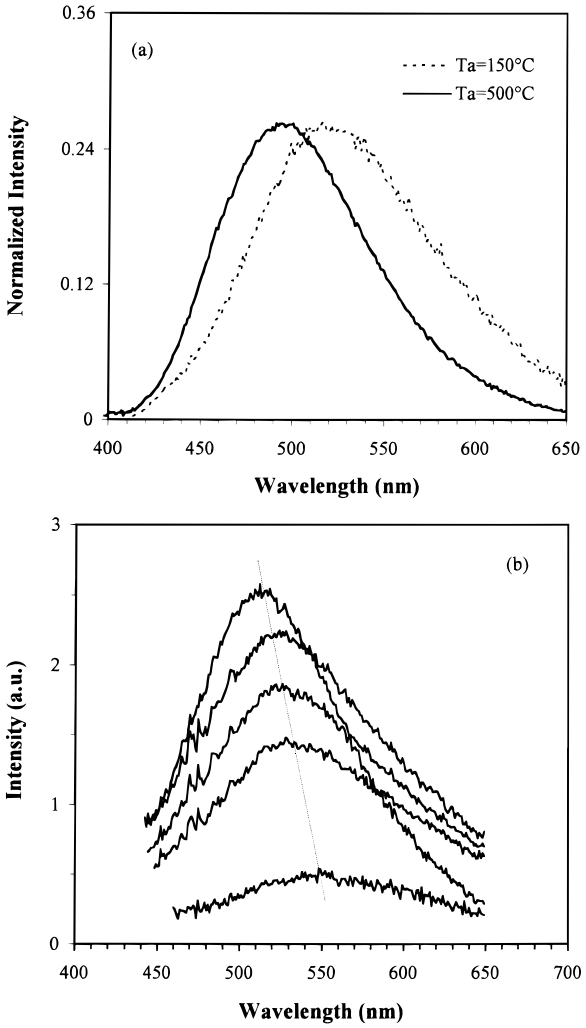

Figure 5. (a) Fluorescence spectra of the exciplex on different silica surfaces. (b) Red shift of the exciplex emission with the increasing coadsorption of MeOH. [MeOH] = 0, 0.6, 1.0, 2.5 monolayer equivalent, and fully condensed in the pores.

II. Exciplex Formation on Silica Surfaces. It is well established in liquid solutions that quenching of the pyrene singlet excited state by DMA occurs in an encounter via electron-transfer interaction which leads to the formation of an CT complex between pyrene and DMA in the excited state, i.e., exciplex. Such an exciplex is conventionally treated as a mixing of a contact ion pair (CIP) state ($Py^{\bullet-}DMA^{\bullet+}$) and a local excited (LE) state ($^1Py^*DMA$).[31] For the reasons given in the following, the pyrene−DMA exciplex has a very high CT character in liquid solutions and also on silica surfaces. Therefore, it can be well approximated by a pure contact ion pair, which is denoted as $^1(Py^{\bullet-}DMA^{\bullet+})^*$, to differentiate from the ground-state CT complex $^1(Py^{\bullet-}DMA^{\bullet+})$. Figure 5a shows

the exciplex emission spectra on fully hydroxylated ($T_a = 150$ °C) and partially dehydroxylated ($T_a = 500$ °C) surfaces. The former exhibits a maximum position at 518 nm and the latter at 490 nm. The blue shift reflects the change of the surface environment by dehydroxylation. Similar fluorescence shifts have been reported in various solvents of different dielectric constants and are understood in terms of solvation of a dipolar excited state in a dielectric continuum.[18a,19a,32]

$$\tilde{\nu}_{max} = \tilde{\nu}_{max}(0) - \frac{\Delta\mu^2}{hca^3} f(n,\epsilon) \quad (3)$$

$$f(n,\epsilon) = 2\frac{\epsilon - 1}{2\epsilon + 1} - \frac{n^2 - 1}{2n^2 + 1} \quad (4)$$

A linear relationship between the spectral maxima and the solvent function $f(n,\epsilon)$ was indeed found for the $^1(Py^{\bullet-}DMA^{\bullet+})^*$ exciplex, and a dipole moment ($\Delta\mu$) larger than 10 D was estimated from eq 3. Similarly, a dipole moment of 15 D was reported for the anthracene−DMA exciplex by using the above solvent shift method.[33] These large dipole moments are indicative of nearly complete electron transfer from DMA to aromatic molecules.[8a,18a] Recent studies of the electronic structure of exciplexes suggest that an exciplex can be considered to be essentially a pure ion pair when its emission maximum is lower in energy that the 0,0 transition of the acceptor excited singlet state by 5000 cm^{-1}.[6] The above criterion substantiates the application of the standard solvent shift analysis to the pyrene−DMA exciplex, since the exciplex has more than 90% ion pair content.

In comparison with the spectral shift data in solutions, the silica surface acts like acetone ($\epsilon = 20.7$) when treated at 150 °C, and it is more like chlorobenzene ($\epsilon = 5.62$) when treated at 500 °C. This is in contradiction with the optical and dielectric measurements of silica gel. The refractive index of silica is well-known, by various techniques, with a value of n =1.4−1.6 and a dielectric constant around $\epsilon = 3.2-3.8$.[34,35] These discrepancies show that it is no longer valid to treat such a two-phase heterogeneous system simply as a continuum dielectric medium.

The decay of the exciplex measured by the time-resolved fluorescence technique exhibits a nonexponential pattern. Such nonhomogeneous decays are often observed on silica surfaces, and Gaussian kinetics are used to describe the effect of site heterogeneity on excitation relaxation.[15] The average fluorescence lifetime of the exciplex from the above Gaussian model is 38 ns on the surface activated at 150 °C , and it is 52 ns on the 500 °C treated surface. The quantum yields of exciplex emission are 0.029 and 0.056, respectively, on these two different surfaces. A comparison with the lifetime and quantum yield data compiled for the exciplex in various solvents shows no consistent analogy between silica and liquid solutions.[19] The fluorescence lifetimes, on one hand, suggest that silica surfaces activated at 150 and 500 °C correspond to solvents with dielectric constants of 11.3 and 10.2, respectively. On the other hand, the quantum yield measurements show that the two different surfaces act like solvents with dielectric constants of 16.5 and 12.3, respectively.

The above results clearly show that the pyrene−DMA exciplex on silica surface has unique spectroscopic properties. In this work, an attempt is made to understand the photophysical and photochemical processes involved in the formation and relaxation of the exciplex on silica surfaces using the electron-transfer theory developed from studies in condensed phases. The following kinetic scheme has been proposed for the formation of exciplex from fluorescence quenching in the liquid phase.[6,16] Diffusion leads to the formation of a reaction encounter between $^1Py^*$ and DMA. A subsequent electron-transfer reaction occurs favorably (i.e., $-\Delta G_{et} \approx \lambda$) with a rate on the order of 10^{11} s^{-1}, which leads to immediate quenching of the pyrene excited state and to formation of an encounter ion pair with a relatively loose structure. Further complexation within the encounter ion pair gives rise to the exciplex. Recent studies of exciplex formation from bimolecular quenching reaction and direct excitation of the ground-state CT complex found that the efficiency (denoted as α) of exciplex formation from the encounter ion pair is unity even in polar liquids, i.e., $\alpha = 1$.[6] Direct formation of a solvent-separated ion pair from the encounter ion pair is insignificant in most liquids, even including polar solvents such as alcohols. The same is true for the pyrene−DMA system on silica surfaces.

$$\underset{\text{reaction encounter}}{^1Py^* + DMA \rightarrow \; [^1Py^{*}\cdots DMA]} \rightarrow \underset{\text{encounter ion pair}}{^1[Py^{\bullet-}\cdots DMA^{\bullet+}]} \xrightarrow{\alpha=1} \underset{\text{exciplex}}{^1(Py^{\bullet-}DMA^{\bullet+})^*} \quad (5)$$

Further deactivation of the exciplex can take place in several different ways, radiatively and nonradiatively, including fluorescence emission, internal conversion to the ground state via back electron transfer, intersystem crossing to give of pyrene triplet excited state (also one type of back electron transfer), and dissociation into ionic products. These processes are clearly shown in the following kinetic scheme.

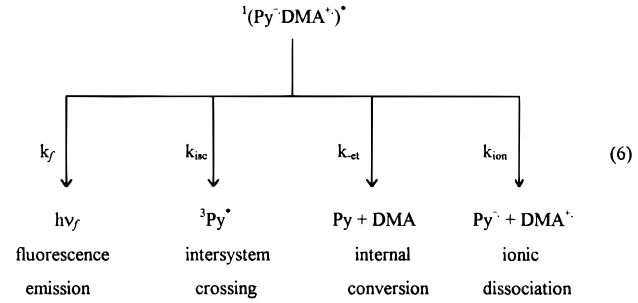

(6)

The decay rate k_{ex} and the fluorescence quantum yield (Φ_f) of the exciplex can be simply defined according to the above scheme.

$$k_{ex} = k_f + k_{isc} + k_{-et} + k_{ion} \quad (7)$$

$$\Phi_f = k_f/k_{ex} = k_f\tau \quad (8)$$

The average decay rate and lifetime of the exciplex from Gaussian kinetics are used in our calculation. Radiative decay rates k_f are estimated to be 7.63×10^5 and 1.08×10^6 s^{-1} respectively on two different surfaces pretreated at 150 and 500 °C (Table 1).

Recent progress in electron-transfer studies found that the fluorescence emission of an exciplex, like the absorption of a ground-state CT complex, is a photoassisted electron-transfer process.[2,5,6] By extending his successful semiclassical approach to thermal ET reactions, Marcus has shown that the structureless CT absorption and exciplex emission spectra are defined by the same energy gap laws for the forward and backward ET, with absorbed and emitted photons included in the energy conservation. The energy at the midpoint between the two mirror-imaged absorption and emission spectra corresponds to the free energy for the return ET process, $-\Delta G_{-et}$, while the

TABLE 1: Quantum Yields of the Exciplex Relaxation Processes and Related Electron-Transfer Parameters for Contact Ion Pair $Py^{\bullet-}$ $DMA^{\bullet+}$ on the Surfaces of Silica Gel M100 Pretreated at Two Different Temperatures

	$T_a = 500$ °C	$T_a = 150$ °C			
	in vacuum	in vacuum	[MeOH] = 1.0 layer	[MeOH] = 2.5 layers	MeOH filled
λ_{max} (nm)	490	518	525	535	552
$-\Delta G_{-et}$ (eV)	3.02	2.95	2.92	2.91	2.87
λ_s (eV)	0.20	0.27	0.29	0.31	0.35
Φ_f	0.056	0.029	0.023	0.014	~0.003
Φ_T	0.12	0.17	0.19	0.25	0.38
Φ_{ion}	0.05	0.08	0.12	0.21	0.48
k_{ex} (s^{-1})	1.92×10^7	2.63×10^7	3.47×10^7	4.79×10^7	3.02×10^8
k_{-et} (s^{-1})	1.49×10^7	1.90×10^7	2.31×10^7	2.52×10^7	4.14×10^7
k_{isc} (s^{-1})	2.30×10^6	4.47×10^6	6.59×10^6	1.20×10^7	1.15×10^8
k_{ion} (s^{-1})	9.59×10^4	2.10×10^5	4.16×10^6	1.01×10^7	1.45×10^8

Stokes shift gives the reorganization energy λ according to the following equations.[2]

$$-\Delta G_{-et} = (hc/2)(\tilde{\nu}_{abs}^{max} + \tilde{\nu}_{em}^{max}) \quad (9)$$

$$\lambda = (hc/2)(\tilde{\nu}_{em}^{max} - \tilde{\nu}_{em}^{max}) \quad (10)$$

Here, $\tilde{\nu}_{abs}^{max}$ and $\tilde{\nu}_{em}^{max}$ are the maxima of the CT absorption and exciplex emission spectra. From the above two equations, the spectral shift of the exciplex emission can be understood in terms of ET parameters.

$$hc\tilde{\nu}_{em}^{max} = -\Delta G_{-et} - \lambda \quad (11)$$

where the total reorganization energy λ includes contributions from a vibrational reorganization λ_v and a solvent or media reorganization λ_s.

$$\lambda = \lambda_v + \lambda_s \quad (12)$$

Since the exciplex formed via bimolecular quenching has the same structure as the one from direct excitation of the ground-state CT complex,[6] the above quantitative relations are used to describe the pyrene−DMA exciplex emission in this work.

There is indeed a weak CT complex between pyrene and DMA in the ground state with an equilibrium constant of 0.23 M^{-1}.[36] The energy of its absorption maximum is estimated to be $h\tilde{\nu}_{abs}^{max} = 3.5$ eV in various hydrocarbons. The solvent shift of the CT absorption spectrum is insignificant mainly due to the cancellation between the solvation stabilization of the exciplex and the solvent reorganization required to carry out the electron transfer. The same absorption maximum at 3.5 eV is used to calculate the ET parameters for the pyrene−DMA charge-transfer system on silica surfaces according to eqs 9 and 10. On the fully hydroxylated surface, the driving force for the back ET is estimated to be $-\Delta G_{-et} = 2.95$ eV, and the total reorganization energy is $\lambda = 0.55$ eV. These values are compared with $-\Delta G_{-et} = 3.18$ eV and $\lambda = 0.32$ eV in *n*-hexane. The stabilization of the exciplex by an additional 0.23 eV on the surface might be attributed to the strong adsorption of ionic species, particularly the cation radical $DMA^{\bullet+}$. If we consider that the vibrational reorganization energy λ_v is around 0.28 eV for the back ET within the ion pair of $Py^{\bullet-}$ and $DMA^{\bullet+}$,[8] the silica support contributes $\lambda_s = 0.27$ eV of the total reorganization energy. Removal of about half of the surface hydroxyl groups by drying the silica at 500 °C results in an increase in the driving force, $-\Delta G_{-et} = 3.02$ eV, and a decrease in λ, i.e., $\lambda = 0.48$ eV. Such changes indicate that surface hydroxyls are the major factor in controlling the energetics of the ET reaction in the adsorbed state. Dehydroxylation leads to a weaker adsorption of the exciplex on the surface and a more rigid environment as characterized by a significantly lower media reorganization energy $\lambda_s = 0.20$ eV. Different from the solvation effect on the energetics of ET in liquid solutions, the reaction between $Py^{\bullet-}$ and $DMA^{\bullet+}$ is greatly influenced by the adsorption of $DMA^{\bullet+}$ on silica surfaces. Solid bulk does not play a major role here due to its rigidity and low dielectric constant. However, ET in silica seems to exhibit a common feature as those in liquids; that is, a stronger interaction between an ion pair and a medium implies a larger reorganization of the environment.

When cyclohexane is coadsorbed onto the silica surfaces, the exciplex emission shifts to the longer wavelength, indicative of a solvation of the exciplex in its adsorbed state. The maximum red shift is only ~0.07 eV, i.e., the limit of extra solvation that cyclohexane can provide for the surface bound exciplex. Figure 5b shows a continual red shift of the exciplex emission with the addition of MeOH vapor to a pyrene and DMA loaded silica sample (T_a = 150 °C). A continuous decrease in the exciplex lifetime is also observed simultaneously with the drop of its fluorescence quantum yield. Exciplex formation gradually moves from the surface region to the liquid confined in nanometer-sized pores when the amount of adsorbed MeOH increases from less than a monolayer to completely filling the porous structure.

III. Charge Separation on Silica Surfaces. Two of the three nonradiative relaxation processes of the exciplex, namely intersystem crossing to a triplet excited state and dissociation into free ion radicals, can be measured directly by transient absorption spectroscopy. Figure 6a shows the transient absorption spectra of a pyrene and DMA loaded silica sample (T_a = 150 °C) in vacuum and with 2.5 monolayers equivalent of MeOH adsorbed on the surface, respectively. To avoid the two-photon ionization of pyrene, the laser beam is only moderately focused onto the silica sample in the diffuse transmittance setup. A higher loading of pyrene, typically 4.0×10^{-7} mol/g, is used to increase the signal/noise ratio. Three absorption bands are identified in the evacuated sample with their maxima at 410, 465, and 515 nm. The two bands at 410 and 515 nm are also observed in the sample loaded with the same amount of pyrene but without DMA, and they are assigned to the T_1-T_n transition of the pyrene triplet state $^3Py^*(T_1)$. The other transient band at 465 nm is attributed to $DMA^{\bullet+}$ by comparison with the well-documented spectrum in liquid solutions and on silica surfaces.[37]

It is reasonable to expect that free radical ions from the ionic dissociation of the exciplex, i.e., $Py^{\bullet-}$ and $DMA^{\bullet+}$, are produced in pairs. As a result, a distinct pyrene anion band should be observed around 490 nm due to its much higher extinction coefficient than that of the DMA cation. However, the pyrene anion is missing in the transient spectrum taken at 100 ns after the laser excitation. Similar transient absorption measurements of porous alumina and zeolite X (K^+ ion exchanged) in a diffuse reflectance setup clearly identified the production of pyrene anion from the DMA quenching of the pyrene fluorescence (data

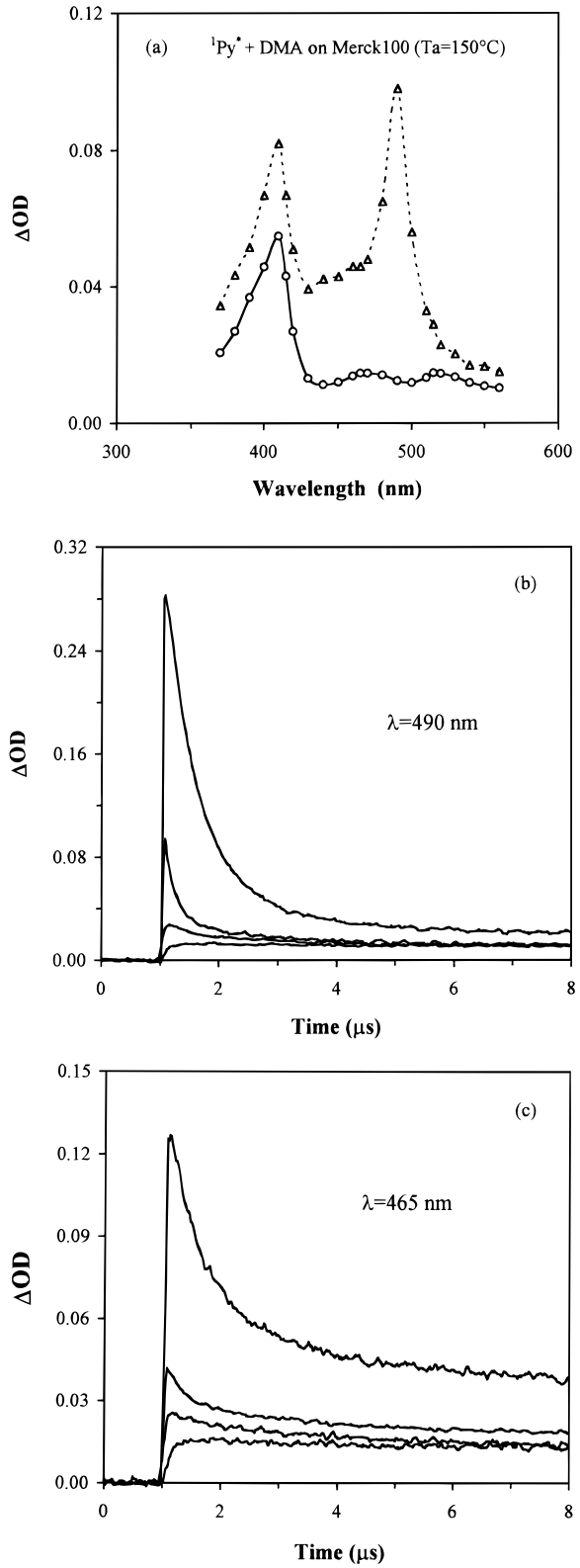

Figure 6. (a) Transient absorption spectra of a laser-irradiated silica sample in vacuum (solid line) and with 2.5 monolayer equivalent MeOH adsorbed (dash line). [Py] = 4.0×10^{-7} mol/g, [DMA] = 1.0×10^{-4} mol/g, T_a = 150 °C. (b) Variation of transient absorption decay traces monitored at 490 nm with increasing loading of MeOH. [MeOH] = 0, 1.0, and 2.5 monolayer equivalent and fully condensed in the pores. (c) Variation of transient absorption decay traces monitored at 465 nm with increasing loading of MeOH. [MeOH]: as the above.

not shown here). The disappearance of the pyrene anion on the silica surface is also in agreement with the recent radiation chemical studies where $Py^{\bullet-}$ is produced in alumina and zeolites but not in silica.[37,38] The higher electron affinity of silica compared to those of arene molecules such as pyrene is inferred. This is supported by data in the literature,[39] where EA(SiO_2) = 0.9 eV as compared to EA(Py) = 0.57 eV. Therefore, it is concluded that the unstable nature of $Py^{\bullet-}$ on silica surface results from its electron-transfer reaction with silica.

$$Py^{\bullet-} + SiO_2 \xrightarrow{k} Py + e_{tr}^- \qquad (13)$$

Electrons trapped in silica e_{tr}^- have been suggested by previous experiments such as photoionization and charge buildup.[30c,40,41] In this case, silica is not an inert solid support any more. It participates in adsorbate reactions as a moderate electron acceptor. The structure of e_{tr}^- and the exact mechanism of the above reaction are not clear at this stage.

Taking the known values of the extinction coefficients of $^3Py^*$ and $DMA^{\bullet+}$ from the literature and using the pyrene triplet yield in a DMA-free silica sample as a standard, i.e., $\Phi_T = 0.22$,[25] the quantum yields of the transient products on a fully hydroxylated surface are estimated to be $\Phi_T = 0.17$ for $^3Py^*$ and $\Phi_{ion} = 0.08$ for $DMA^{\bullet+}$ with every $^1Py^*$ being quenched by DMA. The same transient species are also observed on the partially dehydroxylated surface (T_a = 500 °C). The yields are measured to be $\Phi_T = 0.12$ and $\Phi_{ion} = 0.05$, and no pyrene anion is observed on this surface. From the quantum yields and the exciplex lifetimes, the rates of intersystem crossing and ionic dissociation can be estimated using the following equations.

$$k_{isc} = \Phi_T/\tau \qquad (14)$$

$$k_{ion} = \Phi_{ion}/\tau \qquad (15)$$

The values of these rates are also listed in Table 1. It is noted that a larger ion separation rate is observed on the fully hydroxylated surface. Such low yields of ions indicate that silica is not a useful media for efficient charge separation as compared with polar solvents such as acetone and alcohols. Its charge separation capability is limited by the following two major factors. First of all, the ion pair is only partially "solvated" by the surface, and ion radicals within the pair are strongly bound by the mutual Coulombic interaction through the vacuum space. Unlike the formation of solvent-separated ion pairs in polar liquids, there are no solvent molecules available to move into the space between the two oppositely charged ion radicals and shield the Coulombic interaction. Second, the mobility of ions is low on silica surfaces due to the stronger adsorption of ionic species. Previous work on charge recombination within geminate ion pairs shows that the free ion yield in a system is dependent on the diffusion rate of the two ions within a geminate pair, particularly when the recombination reaction is not diffusion limited.[42] The faster the ionic species move in the system, the higher the yield of free ions results from the dissociation of the geminate pair. For the contact ion pair $Py^{\bullet-}DMA^{\bullet+}$ in our studies, the rate of charge recombination is around $(2.0-2.5) \times 10^7$ s^{-1}, which is much slower than the collision rate as observed for the $^1Py^* + DMA$ reaction, which gives enough time for $Py^{\bullet-}$ and $DMA^{\bullet+}$ to escape. The slow ionic dissociation rates on both surfaces suggest that less mobile ion radicals are strongly held by the electrostatic interaction within the pair.

Coadsorption of a polar solvent such as methanol tends to decrease the lifetime of the exciplex and facilitate the ionic dissociation. The increased ion yields with the adsorption of 2.5 monolayers equivalent of MeOH onto the silica surface (T_a = 150 °C) are shown in Figure 6a. It is particularly interesting to see a new strong band at 490 nm emerging with the addition of MeOH to the system. This is assigned to the pyrene anion

radical based on the same spectrum observed in liquid methanol. The ratio of the intensities of the DMA cation band at 465 nm and the pyrene anion band at 490 nm is reminiscent of the one-to-one correspondence as we expect from the pair dissociation. Figure 6b,c illustrates the variation of the initial yields and kinetic traces of $Py^{\bullet-}$ and $DMA^{\bullet+}$ with the addition of MeOH. The yields of both ions increase gradually with the increasing amount of MeOH present on the silica surface, i.e., from $\Phi_{ion} = 0.08$ on the dry surface ($T_a = 150$ °C) to $\Phi_{ion} = 0.21$ on a wet surface with 2.5 monolayers equivalent of MeOH (see Table 1). The faster decay of the ion signals at lower levels of MeOH adsorption is due to the enhanced ion recombination when the system is changing from a three-dimensional reaction to a two-dimensional one. When the 100 Å silica pores are completely filled with MeOH via capillary condensation of saturated MeOH vapor, the yield and decay rate of ion radicals are about the same as in liquid methanol, i.e., $\Phi_{ion} = 0.48$. Comparison between the decay traces between $Py^{\bullet-}$ and $DMA^{\bullet+}$ indicates that pyrene anion decays slightly faster than the DMA cation, particularly at lower degrees of MeOH adsorption. Even though the initial yields of both ions measured at 20 ns after the laser excitation are about equal in the presence of MeOH, there is always more $DMA^{\bullet+}$ observed than $Py^{\bullet-}$ after the first 2 μs. These observations give more evidence in support of reaction 13.

Quantum yields and rates of the exciplex decay processes and energetic parameters for the back-ET reaction in the presence of MeOH are estimated using the method developed earlier in this work (Table 1). The increase in both k_{-et} and k_{isc} with the decreasing driving force ($-\Delta G_{-et}$) clearly shows an inverted region behavior for the charge recombination reactions. Meanwhile, the increasing production of ion radicals in silica is clearly associated with the extra solvation and the ease of diffusive movement provided by the coadsorbed MeOH. It is concluded from this study that silica surfaces do not constitute favorable environments for charge separation.

Acknowledgment. The authors thank the NATO and the National Science Foundation for financial support of this work.

References and Notes

(1) (a) Marcus, R. A.; Sutin, N. *Biochim. Biophys. Acta* **1985**, *811*, 265. (b) Bolton, J. R., Mataga, N., McLendon, G., Eds. *Adv. Chem. Ser.* **1991**, *228*.

(2) (a) Marcus, R. A. *J. Phys. Chem.* **1989**, *93*, 3078. (b) Marcus, R. A.; Siddarth, P. In *Photoprocesses in Transition Metal Complexes, Biosystems and Other Molecules: Experiment and Theory*; Kochanski, E., Ed.; Kluwer Publishing: Boston, MA, 1992.

(3) (a) Miller, J. R.; Calcaterra, L. T.; Closs, G. L. *J. Am. Chem. Soc.* **1984**, *106*, 3047. (b) Miller, J. R.; Beitz, J. V.; Huddleson, R. K. *J. Am. Chem. Soc.* **1984**, *106*, 5057.

(4) (a) Miller, J. R.; Peeples, J. A; Schmitt, M. J.; Closs, G. L. *J. Am. Chem. Soc.* **1982**, *104*, 6488. (b) Miller, Beitz, J. V. *J. Chem. Phys.* **1981**, *74*, 6746.

(5) (a) Gould, I. R.; Moody, R. E.; Farid, S. *J. Am. Chem. Soc.* **1988**, *110*, 7242. (b) Gould, I. R.; Young, R. H.; Moody, R. E.; Farid, S. *J. Phys. Chem.* **1991**, *95*, 2068. (c) Gould, I. R.; Noukakis, D.; Gomez-Jahn, L.; Young, R. H.; Goodman, J.; Farid, S. *Chem. Phys.* **1993**, *176*, 439.

(6) (a) Gould, I. R.; Young, R. H.; Mueller, L. J.; Farid, S. *J. Am. Chem. Soc.* **1994**, *116*, 8176. (b) Gould, I. R.; Young, R. H.; Mueller, L. J.; Albrecht, A. C.; Farid, S. *J. Am. Chem. Soc.* **1994**, *116*, 8188.

(7) (a) Asahi, T.; Mataga, N. *J. Phys. Chem.* **1989**, *93*, 6575. (b) Ojima, S.; Miyasaka, H.; Mataga, N. *J. Phys. Chem.* **1990**, *94*, 7534. (c) Asahi, T.; Mataga, N. *J. Phys. Chem.* **1991**, *95*, 1956. (d) Asahi, T.; Ohkohchi, M.; Mataga, N. *J. Phys. Chem.* **1993**, *97*, 13132.

(8) (a) Syage, J. A.; Felker, P. M.; Zewail, A. H. *J. Chem. Phys.* **1984**, *81*, 2233. (b) Castella, M.; Prochorow, J.; Tramer, A. *J. Chem. Phys.* **1984**, *81*, 2511. (c) van Dantzig, N. A.; Shou, H.; Alfano, J.; Yang, N. C.; Levy, D. H. *J. Chem. Phys.* **1994**, *100*, 7068. (d) Jortner, J.; Bixon, M.; Wegewjis, B.; Verhoeven, J. W.; Rettschnick, R. P. H. *Chem. Phys. Lett.* **1993**, *205*, 451.

(9) (a) Zhang, G.; Thomas, J. K. *J. Phys. Chem.* **1996**, *100*, 11438. (b) Kira, A. *J. Phys. Chem.* **1981**, *85*, 3047.

(10) (a) Gratzel, M.; Kozak, J. J.; Thomas, J. K. *J. Chem. Phys.* **1975**, *62*, 1632. (b) Thomas, J. K.; Piciulo, P. *J. Am. Chem. Soc.* **1978**, *100*, 3239. (c) Atik, S. S.; Thomas, J. K. *J. Am. Chem. Soc.* **1981**, *103*, 3550.

(11) (a) Kalyanasundaram, K. *Photochemistry in Microheterogeneous Systems*; Plenum Press: New York, 1987. (b) *Photochemistry in Organized and Constraint Media*; Ramamurthy, V., Ed.; VCH: New York, 1991.

(12) (a) Sankaraman, S.; Yoon, K. B.; Yabe, T.; Kochi, J. K. *J. Am. Chem. Soc.* **1991**, *113*, 1419. (b) Yoon, K. B.; Huh, T. J.; Corbin, D. R.; Kochi, J. K. *J. Phys. Chem.* **1993**, *97*, 6492. (c) Yoon, K. B.; Hubig, S. M.; Kochi, J. K. *J. Phys. Chem.* **1994**, *98*, 3865.

(13) Miyasaka, H.; Kotani, S.; Itaya, A. *J. Phys. Chem.* **1995**, *99*, 5757.

(14) (a) Thomas, J. K. *J. Phys. Chem.* **1987**, *91*, 267. (b) Thomas, J. K. *Chem. Rev. (Washington, D.C.)* **1993**, *93*, 301.

(15) Krasnansky, R.; Koike, K.; Thomas, J. K. *J. Phys. Chem.* **1990**, *94*, 4521.

(16) (a) Bauer, R. K.; Borenstein, R.; de Mayo, P.; Okada, K.; Rafalska, M.; Ware, W. R.; Wu, K. C. *J. Am. Chem. Soc.* **1982**, *104*, 4635. (b) Turro, N. J.; Zimmt, M. B.; Gould, I. R. *J. Am. Chem. Soc.* **1985**, *107*, 5826. (c) Marro, M. A. T.; Thomas, J. K. *J. Photochem. Photobiol. A: Chem.* **1993**, *72*, 251.

(17) (a) Turro, N. J.; Cheng, C. C.; Mahler, W. *J. Am. Chem. Soc.* **1984**, *106*, 5022. (b) Turro, N. J. *Tetrahedron* **1987**, *43*, 1589.

(18) (a) Beens, H.; Knibbe, H.; Weller, A. *J. Chem. Phys.* **1967**, *47*, 1183. (b) Knibbe, H.; Rollig, K.; Schafer, F. P.; Weller, A. *J. Chem. Phys.* **1967**, *47*, 1184.

(19) (a) Mataga, N.; Okada, T.; Yamamoto, N. *Chem. Phys. Lett.* **1967**, *1*, 119. (b) Masuhara, H.; Hino, T.; Mataga, N. *J. Phys. Chem.* **1975**, *79*, 994. (c) Hino, T.; Akazawa, H.; Masuhara, H.; Mataga, N. *J. Phys. Chem.* **1976**, *80*, 33. (d) Nishimura, T.; Nakashima, N.; Mataga, N. *Chem. Phys. Lett.* **1977**, *46*, 334. (e) Hirata, Y.; Kanda, Y.; Mataga, N. *J. Phys. Chem.* **1983**, *87*, 1659.

(20) Katusin-Razem, B.; Wong, M.; Thomas, J. K. *J. Am. Chem. Soc.* **1978**, *100*, 1679.

(21) Kano, K.; Kawazumi, H.; Ogawa, T.; Sunamoto, J. *J. Phys. Chem.* **1981**, *85*, 2204.

(22) Birenbaum, H.; Avnir, D.; Ottolenghi, M. *Langmuir* **1989**, *5*, 48.

(23) Iler, R. K. *The Chemistry of Silica: Solubility, Polymerization, Colloid and Surface Properties, and Biochemistry*; John Wiley & Sons: New York, 1979.

(24) Zhang, G. Radiation Induced Processes in Polymer Films and on Silica Surfaces. Ph.D. Dissertation, University of Notre Dame, Notre Dame, IN, 1996.

(25) Ruetten, S. A.; Thomas, J. K. Submitted to *J. Phys. Chem.*

(26) (a) Pankasem, S.; Thomas, J. K. *J. Phys. Chem.* **1991**, *95*, 6990. (b) Kessler, R. W.; Wilkinson, F. *J. Chem. Soc., Faraday Trans. 1* **1981**, *77*, 309. (c) Wilkinson, F.; Willsher, C. J. *Chem. Phys. Lett.* **1984**, *104*, 272.

(27) Owen, C. S. *J. Chem. Phys.* **1975**, *62*, 3204.

(28) Freeman, D.; Doll, J. D. *J. Chem. Phys.* **1983**, *78*, 6002.

(29) Caruso, F.; Grieser, F.; Thistlewaite, P.; Urquhart, R.; Almgren, M.; Wistus, E. *J. Am. Chem. Soc.* **1991**, *113*, 4838.

(30) (a) Bjarneson, D. W.; Peterson, N. O. *J. Am. Chem. Soc.* **1990**, *112*, 988. (b) Oelkrug, D.; Uhl, S.; Wilkinson, F.; Willsher, C. J. *J. Phys. Chem.* **1989**, *93*, 4551. (c) Worrall, D. R.; Williams, S. L.; Wilkinson, F. *J. Phys. Chem. B* **1997**, *101*, 4709.

(31) (a) Mulliken, R. S.; Person, W. B. *Molecular Complexes*; Wiley-Interscience: New York, 1969. (b) Beens, H.; Weller, A. In *Organic Molecular Photophysics*; Birks, J. B., Ed.; Wiley-Interscience: New York, 1975; Vol. II, Chapter 4.

(32) (a) Lippert, E. *Z. Naturforsch.* **1955**, *10A*, 541. (b) Lippert, E. *Electrochem.* **1957**, *61*, 1962. (c) Mataga, N.; Kaifu, Y.; Koizumi, M. *Bull. Chem. Soc. Jpn.* **1956**, *29*, 465.

(33) Okada, T.; Fujita, T.; Kubota, M.; Masaki, S.; Mataga, N.; Ide, R.; Sakata, Y.; Misumi, S. *Chem. Phys. Lett.* **1972**, *14*, 563.

(34) (a) *American Institute of Physics Handbook*, 3rd ed.; American Institute of Physics, McGraw-Hill: New York, 1972. (b) *CRC Handbook of Chemistry and Physics*, 72nd ed.; CRC: Boca Raton, FL, 1991−1992.

(35) Kavanaugh, R. J.; Iu, K.-K.; Thomas, J. K. *Langmuir* **1992**, *8*, 3008.

(36) Yoshihara, K.; Futamura, K.; Nagakura, S. *Chem. Lett.* **1972**, *12*, 1243.

(37) Zhang, G.; Thomas, J. K. *J. Phys. Chem. B* **1997**, *101*, in press.

(38) (a) Liu, X.; Zhang, G.; Thomas, J. K. *J. Phys. Chem. B* **1997**, *101*, 2182. (b) Zhang, G.; Thomas, J. K. Unpublished results.

(39) Campbell, S. A. *The Science and Engineering of Microelectronic Fabrication*; Oxford University Press: New York, 1996.

(40) (a) Oelkrug, D.; Reich, S.; Wilkinson, F.; Leicester, P. A. *J. Phys. Chem.* **1991**, *95*, 269. (b) Mao, Y.; Thomas, J. K. *Chem. Phys. Lett.* **1994**, *226*, 127.

(41) Vigouroux, J. P.; Durand, J. P.; LeMoel, A.; Le Gressus, C.; Griscom, D. L. *J. Appl. Phys.* **1985**, *57*, 5139.

(42) (a) Hong, K. M.; Noolandi, J. *J. Chem. Phys.* **1978**, *68*, 5163. (b) Noolandi, J. In *Kinetics of Nonhomogeneous Processes*; Freeman, G. R., Ed.; John Wiley & Sons: New York, 1987; Chapter 9.